Fuel 316 (2022) 123341

Contents lists available at ScienceDirect

Fuel

journal homepage: www.elsevier.com/locate/fuel

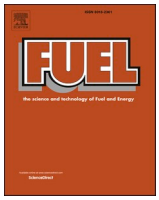

Full Length Article

Cracking of plastic pyrolysis oil over FCC equilibrium catalysts to produce fuels: Kinetic modeling

Roberto Palos *, Elena Rodríguez, Alazne Gutiérrez, Javier Bilbao, José M. Arandes

Department of Chemical Engineering, University of the Basque Country UPV/EHU, PO Box 644, 48080 Bilbao, Spain

ARTICLE INFO

Keywords:
Catalytic cracking
Fuels
Plastic pyrolysis oil
Kinetic model
Deactivation
Waste refinery

ABSTRACT

The kinetics of the catalytic cracking of plastic pyrolysis oil (PPO) over three FCC (fluid catalytic cracking) equilibrium commercial catalysts has been modeled. The PPO comes from the fast pyrolysis of high-density polyethylene (HDPE). The cracking runs have been carried out in a laboratory-scale reactor under FCC conditions: 500–560 °C; catalyst/oil weight ratio of 5 g_{cat} g_{PPO}^{-1}; and contact time of 1.5–6 s. Four different reaction schemes composed of six lumps have been compared and it has been obtained by statistical means that the simplest one is the most appropriate for describing the process. The differences in the kinetic parameters have been related to the properties of the catalysts. Among them, total acidity and mesoporous structure have a key role. The former for promoting the cracking reactions and the latter for limiting the diffusional restrictions of both the bulky compounds within the PPO and the formed coke precursors. This way, ECAT-3 that is the most acid and most mesoporous catalyst, maximizes the yields of naphtha (33.6 wt%) and liquefied petroleum gases (LPG) (18.9 wt%). In contrast, ECAT-1 and ECAT-2 should be chosen for producing light cycle oil (LCO). For ECAT-3, the apparent activation energies of the conversion of heavy cycle oil (HCO) into light cycle oil (LCO), LCO into naphtha, and LCO into LPG are 60.5 42.5 and 58.3 kJ mol^{-1}, respectively. In addition, those of the formation of coke from HCO, LPG and dry gas are 129.0, 4.4 and 40.7 kJ mol^{-1}, respectively.

1. Introduction

The development and wellness of the humankind implies an increase of global pollution. One of the consequences is the increasing presence of waste plastics in the municipal solid wastes (MSW), which overflows the management capability of both public and private entities. Consequently, an unacceptable amount of these wastes ends up landfilled, causing the contamination of the soils and the aquifers [1]. In order to solve these problems, it is well established the interest on tertiary recycling by means of thermochemical processes, i.e. pyrolysis and gasification [2].

The fast pyrolysis of plastics is performed at low temperature, using high heating rates and short residence time for the volatiles. Moreover, it can be carried out in simple and versatile units equipped with different types of reactors (rotary kilns, screw reactors, fluidized or spouted beds, etc.) entailing a reduced environmental impact and with the possibility of tuning the operating conditions to adapt the production to the type of plastic fed [3,4]. The ideal goal of pyrolysis processes is the monomer recovery, which can be done with high yields in the pyrolysis of polystyrene [5] and polymethyl-methacrylate [6]. On the other hand, for polyolefinic plastics, which constitute two thirds of the plastic fraction found in the MSW [7], is of great interest the production of plastic pyrolysis oil (PPO) because of its possibilities to be used as an alternative fuel [8].

Based on its properties, the PPO has been considered as a potential fuel for diesel engines feeding it neatly or blended with commercial diesel [9]. Nevertheless, the PPO does not meet the tough requirements of commercial fuels and requires of physicochemical treatments to adapt its composition [10]. This situation has led to the proposal of integrating the fast pyrolysis of waste plastics with the upgrading of the PPO in refinery units (Waste-Refinery) [11]. The interest of the proposal lays on the capacity of refinery units for valorizing the PPO, either in *ad hoc* catalytic units or in already existing industrial units. The fluid catalytic cracking (FCC) units are the most appropriate ones in the short term, given their high capacity and versatility to manage unconventional feeds, such as diverse secondary refinery streams [12,13] or bio-oil [14]. Indeed, the chemical composition of the PPO (highly olefinic and free of aromatics) makes it appropriate to be fed to catalytic cracking units with the aim of producing fuels free of sulfur and nitrogen [15]. Furthermore, within the facilities available in the refineries, there are the required fractionation and conditioning units to obtain fuels similar to

* Corresponding author.
E-mail address: roberto.palos@ehu.eus (R. Palos).

https://doi.org/10.1016/j.fuel.2022.123341
Received 23 September 2021; Received in revised form 10 January 2022; Accepted 16 January 2022
Available online 1 February 2022

Nomenclature

Abbreviations

C/O	catalyst to oil weight ratio
FBP	final boiling point
FCC	fluid catalytic cracking
HCO	heavy cycle oil
IBP	initial boiling point
LCO	light cycle oil
LPG	liquefied petroleum gases
MSW	municipal solid waste
PPO	plastic pyrolysis oil
SSE	mean squared error
VGO	vacuum gasoil

Symbols

A	correlation coefficient
C	molar concentration (mol cm^{-3})
E	apparent activation energy (kJ mol^{-1})
i	certain lump
j	certain reaction
k	apparent kinetic parameter ($m^6\ kg_{cat}^{-1}\ kmol^{-1}\ s^{-1}$ / $m^3\ kg_{cat}^{-1}\ s^{-1}$)
k_d	catalyst deactivation kinetic parameter (s^{-1})
m	reaction order
M_{HCO}	molecular weight of HCO lump (g mol^{-1})
m_{cat}	mass of catalyst (g)
m_{PPO}	mass of PPO (g)
n_e	number of experiments
n_l	number of lumps
n_p	number of parameters
p	certain experiment
r	reaction rate
R	ideal gas constant (8.314 J $mol^{-1}\ K^{-1}$)
t	contact time (s)
T	reaction temperature (°C)
T*	reference temperature (°C)
V	volume of the reactor (cm^3)
y	weight fraction

Greek symbols

α	level of significance
φ	activity term
υ	stoichiometric coefficient
ν	degrees of freedom

conventional ones. Among the advantages that the Waste–Refinery strategy offers, the following ones must be highlighted: (i) the recycling of petroleum-derived products with the subsequent savings of raw materials; (ii) the removal of economic barriers that entails the design and construction of new units, which correspond to the high cost of the equipment and of the marketing of non-conventional fuels that would compete against the conventional fuels; and, (iii) the rational organization of the plastics recycling, carrying out the pyrolysis process in a delocalized way in units located nearby of the waste plastics collection and segregation points. The PPO would be afterwards transported from different geographical areas to centralized refineries for its large-scale valorization. Feeding a liquid stream, such as the PPO, into a cracking unit, entails less technical difficulties that the feeding of pure polyolefins, the cracking of which has been also studied [16–18]. Nonetheless, these initiatives will require a rigorous control of the feeds, since their composition can be easily contaminated by the presence of different plastics and of additives and pollutants in the waste plastics.

In a previous work it has been studied the effect of the properties of different FCC equilibrium catalysts on the production of fuel from PPO, operating at 500–560 °C and using a riser simulator reactor [19]. Interestingly, the yields of naphtha (highly olefinic and with a high octane rating) and light olefins were superior to 40 and 12 wt%, respectively. The proposed initiative is similar to that of cracking wax from Fischer-Tropsch process with the aim of producing high octane gasoline and light olefins [20,21].

Both for the simulation and optimization of an *ad hoc* designed reactor and for the feeding of the PPO to an industrial FCC unit, it is required a kinetic model capable of quantifying the products distribution. Traditionally, the efforts in the kinetic modeling have been focused on the cracking of vacuum gasoil (VGO). Moustafa and Froment [22] were pioneers in taking into account the heterogeneous composition of the VGO and they proposed a kinetic model with a complex reaction scheme that described the individual reactions involved and the formation of coke by means of elementary steps. This type of molecular-level kinetic models has been also applied for the cracking of wax from Fischer-Tropsch process [21]. Nevertheless, most of the works have established lump-based kinetic models that simplify the computing and their posterior use in the design of the reactor [23–25]. Apart from the complexity of the reaction scheme, an additional difficulty for obtaining kinetic models is the extremely fast deactivation of the catalyst caused by coke deposition [26,27]. Kinetic models for the catalytic cracking of VGO consider between 3 and 17 lumps and have been collected by different authors [28,29]. These models assume that kinetic parameters are apparent values as a consequence of the diffusional restrictions caused by the components of the VGO (especially the heavier ones) [30].

In this work, it has been established a six-lump based kinetic model for the cracking of PPO obtained in the pyrolysis of high-density polyethylene from the experimental data obtained in a previous work [19]. The aim of the work is to provide a tool for quantifying the effects of the operating conditions on the yields of products of interest, such as fuels (gasoline and diesel) and commodities (light olefins). In the modeling, it has been taking into account the catalyst deactivation by coke deposition, which is extremely significant in cracking reactions. Moreover, the analysis of the kinetic parameters obtained for three different FCC equilibrium catalysts with different acidity and porous structure allows for assessing the effect of these properties on the different catalytic steps and on the formation of coke.

2. Material and methods

2.1. Materials

The plastic pyrolysis oil (PPO) has been obtained at 500 °C under fast pyrolysis conditions by feeding virgin high-density polyethylene (HDPE) to a fountain confined conical spouted bed reactor [31].

Three different commercial equilibrium FCC catalysts (ECAT-1, ECAT-2 and ECAT-3) have been used in the work. The catalysts have been collected from the catalyst purge stream of industrial FCC units, specifically ECAT-1 from Petronor Refinery (Spain) and the other catalysts from Petrobras Refinery (Brazil). Consequently, they are equilibrium catalysts, since they have been submitted to numerous cycles composed of reaction, stripping and regeneration steps in their corresponding FCC units [32].

2.2. Experimental setup

The catalytic cracking runs have been performed on a laboratory scale micro-riser reactor, specifically designed to mimic the conditions of the riser reactor of industrial FCC units [33]. A schematic representation of the experimental unit together with an explanation of the experimental procedure can be found elsewhere [34]. The operating conditions of riser simulator reactor have been: temperature, 500, 530 and 560 °C; catalyst to oil weight ratio (C/O), 3–7 g_{cat} g_{PPO}^{-1}; and contact time, 1.5–6 s.

3. Kinetic model

3.1. Model description

The catalytic cracking of the PPO has been described by means of a six-lump reaction network. The six lumps are heavy cycle oil (HCO, C_{20+}), light cycle oil (LCO, C_{13}-C_{20}), naphtha (C_5-C_{12}), liquefied petroleum gases (LPG, C_3-C_4), dry gas (C_1-C_2) and coke (carbonaceous material deposited on the catalyst). The reaction network in Fig. 1a corresponds to parent reaction network and it accounts for sixteen kinetic parameters, to which it must be added a parameter for catalyst deactivation.

3.2. Model equations and methodology

The kinetic modeling methodology used is based on the one developed by Toch et al. [35] for catalytic processes with complex pathways and on that proposed by Cordero-Lanzac et al. [36,37], since they included the catalyst deactivation on it. Furthermore, the methodology has been adapted for handling the experimental data obtained in a batch reactor. Likewise, a molar balance to the micro riser reactor has been also required in order to properly describe the behavior of the different lumps [38]. According to the reaction network in Fig. 1a, the reaction rate equations that describe the evolution with contact time of the different lumps are listed below.

$$\frac{dy_{HCO}}{dt} = -\frac{\varphi\left[\left(\frac{m_{PPO}}{M_{HCO}\,V}\right)(k_1+k_2+k_3+k_4+k_5)\,y_{HCO}^2\right]m_{cat}}{V} \quad (1)$$

$$\frac{dy_{LCO}}{dt} = \frac{\varphi\left[\left(\frac{m_{PPO}}{M_{HCO}\,V}\right)(k_1\,y_{HCO}^2)-(k_6+k_7+k_8+k_9)\,y_{LCO}\right]m_{cat}}{V} \quad (2)$$

$$\frac{dy_{Naphtha}}{dt} = \frac{\varphi\left[\left(\frac{m_{PPO}}{M_{HCO}\,V}\right)(k_2\,y_{HCO}^2)+(k_6\,y_{LCO})-(k_{10}+k_{11}+k_{12})\,y_{Naphtha}\right]m_{cat}}{V} \quad (3)$$

$$\frac{dy_{LPG}}{dt} = \frac{\varphi\left[\left(\frac{m_{PPO}}{M_{HCO}\,V}\right)(k_3\,y_{HCO}^2)+(k_7\,y_{LCO})+(k_{10}\,y_{Naphtha})-(k_{13}+k_{14})\,y_{LPG}\right]m_{cat}}{V} \quad (4)$$

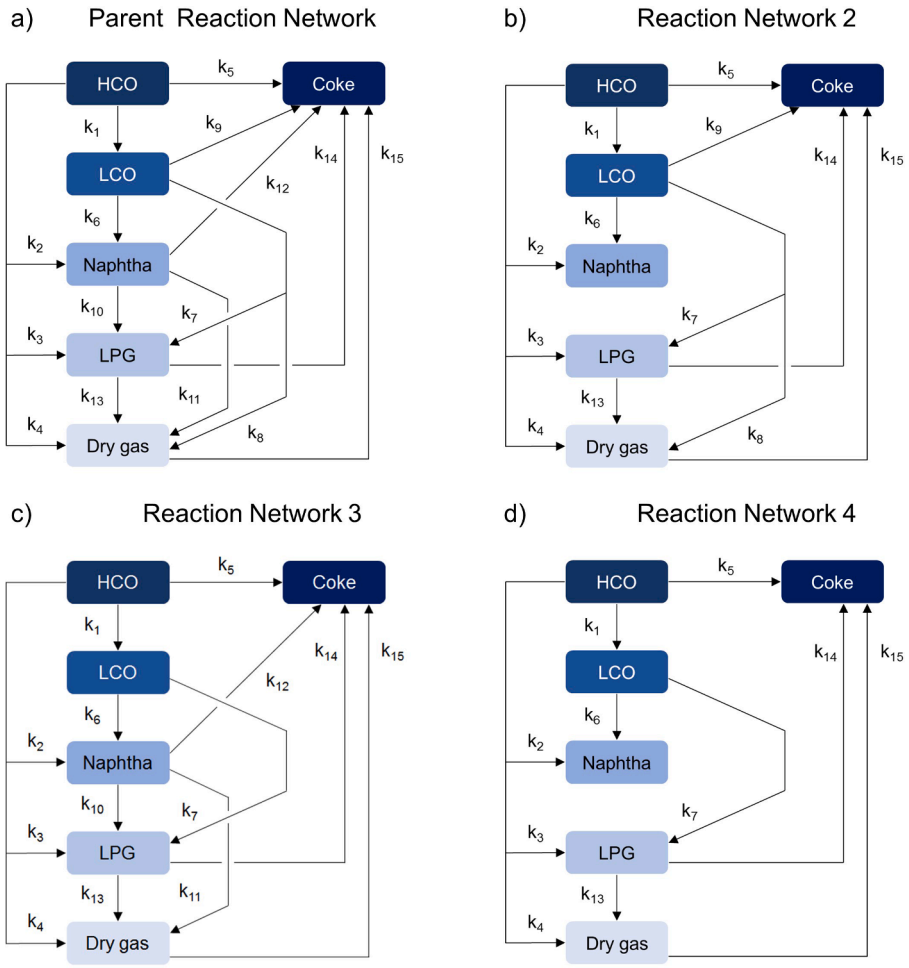

Fig. 1. Proposed reaction networks.

$$\frac{dy_{Dry\ Gas}}{dt} = \frac{\varphi\left[\left(\frac{m_{PPO}}{M_{HCO}\ V}\right)\left(k_4\ y_{HCO}^2\right) + \left(k_8\ y_{LCO}\right) + \left(k_{11}\ y_{Naphtha}\right) + \left(k_{13}\ y_{LPG}\right) - \left(k_{15}\ y_{DryGas}\right)\right] m_{cat}}{V} \quad (5)$$

$$\frac{dy_{Coke}}{dt} = \frac{\varphi\left[\left(\frac{m_{PPO}}{M_{HCO}\ V}\right)\left(k_5\ y_{HCO}^2\right) + \left(k_9\ y_{LCO}\right) + \left(k_{12}\ y_{Naphtha}\right) + \left(k_{14}\ y_{LPG}\right) + \left(k_{15}\ y_{DryGas}\right)\right] m_{cat}}{V} \quad (6)$$

being y_i the weight fraction of lump *i*, t the contact time between the reactants and the catalyst in the reactor, M_{HCO} the molecular weight of the lump HCO, V the volume of the reactor, k_j the apparent rate constant of reaction *j*, m_{PPO} the mass of PPO fed and m_{cat} the mass of catalyst used.

One should observe that the catalytic cracking of the different lumps has been described using irreversible first-order reactions, with the exception of the cracking of HCO lump, which has been considered as an irreversible second-order reaction [28,39]. Additionally, it has been assumed that cracking reactions are non-selectively affected by catalyst deactivation and it has been quantified in Eqs. (1)-(6) by using the same activity term (φ), which has been defined as:

$$\varphi = \frac{(-r_j)}{(-r_j)_0} = \exp\ (-k_d\ t) \quad (7)$$

where $(-r_j)$ and $(-r_j)_0$ are the reaction rates of each step of the reaction network at *t* time and zero time, respectively, and k_d is the deactivation parameter.

The equation proposed for explaining the deactivation kinetics corresponds to a first-order exponential function, which is effective for describing the activity decay in the cracking reactions where a notably deactivation occurs for short contact times (<20 s) [40].

For computing the kinetic parameters, they have been expressed as a function of temperature by means of the reparameterized Arrhenius equation in order to avoid the regression issues derived from the strong correlation between the activation energy and the pre-exponential factor.

$$k_j = k_j^*\ \exp\left[-\frac{E_j}{R}\left(\frac{1}{T} - \frac{1}{T^*}\right)\right] \quad (8)$$

being k_j* the kinetic reaction rate of the *j* reaction step at the reference temperature T* (500 °C), E_j the corresponding apparent activation energy and R the universal gas constant.

The system of differential equations that describes the catalytic cracking of PPO, Eqs. (1)-(6), has been solved using an in-house written MATLAB code. The code estimated the required kinetic rate constants and activation energies to fit the weight fraction of the different parameters to those experimentally obtained. To find the best fitting values, a loss function in which the mean squared error is minimized has been employed.

$$\text{Loss Function} = \frac{1}{n_e} \cdot \sum_{1}^{n_l} \sum_{1}^{p} \left(y_{i,p}^{cal} - y_{i,p}^{exp}\right)^2 \quad (9)$$

where y_{ip} is the weight fraction of lump *i* for experiment *p*, n_l is the total number of lumps and n_e the total number of experiments. Moreover, superscripts "cal" and "exp" denote the calculated and experimentally determined weight fractions, respectively.

3.3. Statistical significance

The discrimination between the different models proposed has been performed by means of a statistical significance test based on Fisher's method. The procedure is well explained in the literature [41]. In brief, for two kinetic models with different degrees of freedom ($\nu_A \neq \nu_B$) if model B shows a smaller mean squared error than model A ($SSE_B < SSE_A$), the improvement offered by model B with respect to model A will be statistically significant when the following condition is fulfilled:

$$F_{A-B} = \frac{\frac{SSE_A - SSE_B}{SSE_B}}{\frac{\nu_A - \nu_B}{\nu_B}} > F_{1-\alpha}(\nu_A - \nu_B, \nu_B) \quad (10)$$

being $F_{1-\alpha}$ the critical value of the Fischer distribution function for a level of significance of 95% (α = 0.05). The degrees of freedom have been computed according to the following equation by taking into account the number of experiments (n_e), number of lumps (n_l) and number of parameters (n_p):

$$\nu = (n_e \cdot n_l) - n_p \quad (11)$$

4. Results

4.1. Characterization

The main properties of the PPO are provided in Table 1. It consists of a mixture of hydrocarbons with a broad distillation range that can be divided into 82.0 wt% of HCO (heavy cycle oil), 12.5 wt% of LCO (light cycle oil) and 5.5 wt% of naphtha. These fractions have been defined according to the usual criteria followed by oil refiners: naphtha (C_5–C_{12}), LCO (C_{13}–C_{20}) and HCO (C_{21+}) [42]. Additionally, the chemical composition of the PPO obtained by chromatographic means has been already reported in our previous work [43]. Briefly, they are composed of 67.6 wt% of olefins and 32.4 wt% of paraffins.

Even though a descriptive characterization of the catalysts has been already reported in a previous work [44], their main properties are shown in Table 2. In order to compare the properties of these industrial catalysts it must be taken into account its complex configuration, which is composed of an ultrastable Y zeolite (USY) embedded in a meso- and macroporous matrix (consisting of a mixture of clay, silica and alumina) [45]. The highest content of zeolite of ECAT-2 (21 wt%) is in concordance with its high micropore surface area (139 $m^2\ g^{-1}$). ECAT-3, in turn, has the highest matrix/USY zeolite ratio, which turns into the highest mesopore surface area and mesopore volume (111 $m^2\ g^{-1}$ and 172 $cm^3\ g^{-1}$, respectively). This way, its wide porous structure increases the accessibility of the NH_3 to the acid sites, making ECAT-3 the catalyst with the highest total acidity (124 $\mu mol_{NH3}\ g^{-1}$), acid strength (130 kJ mol_{NH3}^{-1}) and Brønsted/Lewis acid sites ratio (1.56). Furthermore, the high mesopore volume of the matrix will reduce diffusional constraints

Table 1
Characterization results of the PPO [43].

Physical properties	
Specific gravity (°API)	20.7
Viscosity at 100 °C (cSt)	2.2
Average molecular weight (g mol^{-1})	1430
Simulated distillation (°C)	
IBP-FBP	157–618
T_{50}-T_{95}	472–601

Table 2
Properties of the commercial FCC equilibrium catalysts [44].

	ECAT–1	ECAT–2	ECAT–3
USY zeolite content (wt%)	13.8	21.0	11.8
Zeolite UCS (Å)	24.26	24.23	24.27
Physical properties			
Apparent bulk density (g cm^{-3})	0.90	0.88	0.89
BET surface area (m^2 g^{-1})	124	190	174
Micropore surface area (m^2 g^{-1})	87	139	63
Micropore volume (cm^3 g^{-1})	0.04	0.06	0.03
Mesopore surface area (m^2 g^{-1})	37	50	111
Mesopore volume (cm^3 g^{-1})	112	147	172
Acidic properties			
Acidity (μmol_{NH3} g^{-1})	40	81	124
Average acid strength (kJ mol_{NH3}^{-1})	100	126	130
Brønsted/Lewis acid sites ratio	0.66	0.91	1.56
Chemical composition			
Al_2O_3 (wt%)[a]	53.8	52.2	62.8
SiO_2 (wt%)	38.5	44.0	35.1
SiO_2/Al_2O_3 ratio	0.72	0.84	0.56
Cu (ppm)	24	66	10
Ni (ppm)	741	106	53
V (ppm)	3335	244	67
Fe (wt%)	0.19	0.25	0.21
Na (wt%)	0.29	0.26	0.19
P_2O_5 (wt%)	0.62	0.45	0.32
rare earths (wt%)	2.50	0.86	1.35

[a] Corresponding to the total content of alumina (in zeolite and matrix)

Table 3
Apparent kinetic parameters at the reference temperature and activation energies for the reactions involved in the catalytic cracking of plastic pyrolysis waxes.

Step	Reaction involved	$k_{j,\ 773\ K}$	E_j [d]
–	Deactivation, k_d[a]	$(3.2 \pm 0.2)\ 10^{-2}$	136.0 ± 7.1
1	HCO → LCO, k_1[b]	41.8 ± 2.4	63.6 ± 3.4
2	HCO → Naphtha, k_2[b]	14.4 ± 0.8	86.6 ± 4.1
3	HCO → LPG, k_3[b]	1.4 ± 0.1	17.8 ± 1.1
4	HCO → Dry gas, k_4[b]	0.8 ± 0.2	22.2 ± 1.5
5	HCO → Coke, k_5[b]	2.4 ± 0.1	112.9 ± 5.4
6	LCO → Naphtha, k_6[c]	$(3.5 \pm 0.2)\ 10^{-4}$	96.2 ± 4.8
7	LCO → LPG, k_7[c]	$(3.8 \pm 0.8)\ 10^{-3}$	63.2 ± 3.3
8	LCO → Dry gas, k_8[c]	$(3.3 \pm 0.1)\ 10^{-8}$	56.9 ± 3.4
9	LCO → Coke, k_9[c]	$(3.4 \pm 0.2)\ 10^{-8}$	102.1 ± 5.2
10	Naphtha → LPG, k_{10}[c]	$(3.2 \pm 0.4)\ 10^{-6}$	73.2 ± 3.8
11	Naphtha → Dry gas, k_{11}[c]	$(2.6 \pm 0.4)\ 10^{-6}$	49.8 ± 2.5
12	Naphtha → Coke, k_{12}[c]	$(2.8 \pm 0.6)\ 10^{-9}$	140.6 ± 7.7
13	LPG → Dry gas, k_{13}[c]	$(4.7 \pm 0.9)\ 10^{-3}$	54.4 ± 2.9
14	LPG → Coke, k_{14}[c]	$(5.9 \pm 0.5)\ 10^{-4}$	89.5 ± 4.8
15	Dry gas → Coke, k_{15}[c]	$(1.6 \pm 0.1)\ 10^{-2}$	130.1 ± 6.4

The parameters are measured in: [a] s^{-1}; [b] m^6 kg_{cat}^{-1} $kmol^{-1}$ s^{-1}; [c] m^3 kg_{cat}^{-1} s^{-1}; [d] kJ mol^{-1}

of the long chains of PPO, easing its access to the external crystal surface of zeolites and, consequently, its posterior cracking on the channels of the zeolite.

It is also remarkable the presence of rare earths in the catalysts, especially for ECAT-1 (2.50 wt%), since these elements increase the selectivity to naphtha lump [46]. The presence of P_2O_5 (with a maximum value of 0.62 wt% for ECAT-1) aims the formation of light olefins. Metals, such as V, Fe and Ni, are irreversibly deposited on FCC catalysts in the successive reaction-regeneration cycles acting as poisons and causing a reduction in throughput by increasing coke formation [47].

4.2. Model simplification

In order to validate the model proposed, the results obtained with ECAT-1 for the parent reaction network (Fig. 1a) are shown below. The values of the apparent kinetic rate constants and activation energies that have minimized the mean squared error of the loss function (Eq. (9)) have been collected in Table 3. The values of the parameters provide a large amount of information about the relevancy of the different catalytic steps. This way, it can be seen that the steps that govern the catalytic cracking of PPO are those in which the cracking of HCO fraction is involved (steps #1 to #5 in Fig. 1a). The highest crackability of the compounds within the HCO fraction is a common result obtained in the catalytic cracking of hydrocarbon streams and it is coherent with the higher crackability of the high-molecular weight olefins [25,48]. However, the values of some of the kinetic rate constants, in particular those corresponding to steps #8 to #12, are so small that the contribution of these kinetic steps can be considered negligible.

Therefore, three alternative reaction networks have been proposed (Fig. 1b, c and d) in which various simplifications have been made based on the results collected in Table 3. This way, in alternative network 2 (Fig. 1b) the naphtha fraction has been considered as a final product, i.e. steps #10, #11 and #12 have been removed from the parent network (Fig. 1a). In alternative network 3 (Fig. 1c), in turn, the steps removed have been those in which LCO fraction is converted into coke and into dry gas fractions (steps #8 and #9). Finally, alternative network 4, which is the simplest one from all the proposed, ignores all the routes removed in alternative networks 2 and 3. Thus, in alternative network 4 (Fig. 1d) steps #8 to #12 have been removed from the parent one (Fig. 1a).

Consequently, the fitting of the experimental data obtained for the catalytic cracking of PPO with ECAT-1 has been also performed for the alternative reaction networks. Overall, good fitting results have been obtained for all of them. Hence, in order to perform an appropriate discrimination between the four networks, the statistical significance test based on Fisher's method described in Section 3.3 has been applied. The results obtained have been tabulated in Table 4. Attending to the statistical parameters, it can be seen that the number of experiments and lumps is the same for all the networks, but the number of parameters varies following the trend: $n_{p,1} > n_{p,3} > n_{p,2} > n_{p,4}$. Consequently, the degrees of freedom of the different reaction networks follows just the opposite order. On the other hand, the lowest value for the sum of squared errors has been obtained for scheme 3 ($5.844\ 10^{-3}$), whereas the values obtained for the other networks are slightly higher and follow the trend: $SSE_2 < SSE_1 < SSE_4$. Therefore, since alternative reaction network 4 is the simplest one (less amount of parameters) and the worst fitting has been obtained with it, this one has been taken as reference for the statistical comparison. Thus, it has been assessed if the addition of more catalytic steps is statistically significant. It has been obtained that $F_{4-1} < F_{1-\alpha}$ ($0.841 < 2.259$), $F_{4-2} < F_{1-\alpha}$ ($1.569 < 3.040$) and $F_{4-3} < F_{1-\alpha}$ ($1.569 < 2.649$), meaning that neither parent network nor alternatives 2 and 3 improved in a statistically significant way the fitting of alternative scheme 4.

4.3. Kinetic parameters

Based on all the previous, the alternative reaction network 4 has been also used for the fitting of the data obtained with both ECAT-2 and ECAT-3. The goodness of fit has been evaluated using parity plots

Table 4
Statistical comparison of the four kinetic networks.

Statistical parameter	Reaction network			
	1	2	3	4
n_e	36	36	36	36
n_l	6	6	6	6
n_p	16	13	14	11
ν	200	203	202	205
SSE	$5.851\ 10^{-3}$	$5.848\ 10^{-3}$	$5.844\ 10^{-3}$	$5.974\ 10^{-3}$
F	0.841 (F_{4-P})	1.569 (F_{4-2})	1.569 (F_{4-3})	
$F_{1-\alpha}$	2.259	3.040	2.649	

Table 5
Apparent kinetic parameters at the reference temperature for the reactions involved in the catalytic cracking of PPO for the three catalysts.

Step	Reaction	$k_{i,\ 773\ K}$		
		ECAT-1	ECAT-2	ECAT-3
–	Deactivation, k_d[a]	$(2.4 \pm 0.2)\ 10^{-2}$	$(3.0 \pm 0.2)\ 10^{-2}$	$(2.3 \pm 0.2)\ 10^{-2}$
1	HCO → LCO, k_1[b]	41.1 ± 1.4	42.8 ± 1.8	41.5 ± 1.0
2	HCO → Naphtha, k_2[b]	14.3 ± 1.1	14.7 ± 1.5	14.7 ± 1.7
3	HCO → LPG, k_3[b]	1.42 ± 0.8	1.80 ± 0.6	1.50 ± 0.7
4	HCO → Dry gas, k_4[b]	0.79 ± 0.1	0.72 ± 0.3	1.16 ± 0.5
5	HCO → Coke, k_5[b]	2.08 ± 0.1	2.10 ± 0.2	2.02 ± 0.2
6	LCO → Naphtha, k_6[c]	$(2.4 \pm 0.4)\ 10^{-4}$	$(4.5 \pm 0.3)\ 10^{-4}$	$(1.0 \pm 0.1)\ 10^{-3}$
7	LCO → LPG, k_7[c]	$(3.9 \pm 0.5)\ 10^{-3}$	$(3.8 \pm 0.4)\ 10^{-3}$	$(4.1 \pm 0.6)\ 10^{-3}$
13	LPG → Dry gas, k_{13}[c]	$(4.5 \pm 0.5)\ 10^{-3}$	$(4.9 \pm 0.9)\ 10^{-3}$	$(4.5 \pm 0.4)\ 10^{-3}$
14	LPG → Coke, k_{14}[c]	$(1.7 \pm 0.2)\ 10^{-3}$	$(2.8 \pm 0.7)\ 10^{-3}$	$(1.1 \pm 0.3)\ 10^{-3}$
15	Dry gas → Coke, k_{15}[c]	$(1.9 \pm 0.1)\ 10^{-5}$	$(1.2 \pm 0.3)\ 10^{-4}$	$(4.7 \pm 0.6)\ 10^{-5}$

The parameters are measured in: [a] s^{-1}; [b] $m^6\ kg_{cat}^{-1}\ kmol^{-1}\ s^{-1}$; [c] $m^3\ kg_{cat}^{-1}\ s^{-1}$

(Fig. S1 in the Supplementary Material) by evaluating the final fit of calculated data for the three catalysts against raw experimental data. As it can be seen, almost a perfect fit between the calculated and the experimental weight fraction has been obtained for all the catalysts, with the exception of the scattering of some points, especially for ECAT-3. Nevertheless, those deviations do not exceed the 5% as they remain inside the region delimited by the dashed lines.

In Table 5 have been collected the values computed for the apparent kinetic parameters and the activation energies of the kinetic steps involved in the catalytic cracking of PPO by the three catalysts. Overall, small differences have been obtained in the values of the kinetic parameters with all the catalysts. These differences lie in the properties of the catalysts, considering the effect of the acidity and porous structure on the activity, selectivity and deactivation of the catalysts [49]. This way, ECAT-2 has the highest value for the deactivation parameter ($0.030\ s^{-1}$) because of its moderate mesopore surface area ($50\ m^2\ g^{-1}$) and mesopore volume ($147\ cm^3\ g^{-1}$), which are not enough for easing the diffusion of coke precursors towards the external surface of catalyst particles. Likewise, the confinement of the precursors will block the micropores of the zeolite resulting in the ineffectiveness of its high content of zeolite [50]. It is well-established the role as coke precursors of light olefins in cracking processes, as they undergo oligomerization, aromatization and condensation reactions that are catalyzed by strong acid sites [51,52]. In the same line, do stand out the rate constants of the reactions that form coke from LPG and dry gas fractions ($2.8\ 10^{-3}$ and $1.0\ 10^{-4}\ m^3\ kg_{cat}^{-1}\ s^{-1}$, respectively) using ECAT-2.

Table 6
Values of the apparent activation energy of the reactions involved in the catalytic cracking of PPO for the three catalysts.

Step	Reaction	E_i (kJ mol^{-1})		
		ECAT-1	ECAT-2	ECAT-3
–	Deactivation	163.2 ± 8.0	79.2 ± 3.8	120.3 ± 5.9
1	HCO → LCO, E_1	65.3 ± 3.4	72.8 ± 3.4	60.5 ± 2.7
2	HCO → Naphtha, E_2	97.3 ± 4.8	96.2 ± 4.0	89.4 ± 4.1
3	HCO → LPG, E_3	17.7 ± 1.0	18.4 ± 2.0	16.6 ± 1.3
4	HCO → Dry gas, E_4	21.5 ± 1.1	17.1 ± 1.4	26.8 ± 1.0
5	HCO → Coke, E_5	125.9 ± 6.3	133.0 ± 6.6	129.0 ± 6.0
6	LCO → Naphtha, E_6	122.5 ± 6.0	83.9 ± 4.8	42.5 ± 2.6
7	LCO → LPG, E_7	63.9 ± 3.3	69.4 ± 5.5	58.3 ± 3.1
13	LPG → Dry gas, E_{13}	57.4 ± 2.9	40.0 ± 3.5	72.9 ± 4.0
14	LPG → Coke, E_{14}	31.8 ± 1.4	27.3 ± 1.4	4.4 ± 0.5
15	Dry gas → Coke, E_{15}	105.2 ± 5.2	91.7 ± 4.8	40.7 ± 2.1

In contrast, the lower zeolite/matrix ratio of ECAT-3 that entails a higher mesopore surface area ($111\ m^2\ g^{-1}$) and a higher mesopore volume ($172\ cm^3\ g^{-1}$), will improve the diffusion of coke precursors, attenuating their confinement and, consequently, the blockage of the micropores. Moreover, the enhanced accessibility and diffusion of PPO chains to the active sites in ECAT-3 are in concordance with the high values of the kinetic parameters for the reactions that convert the components within the HCO lump into dry gases ($1.16\ m^6\ kg_{cat}^{-1}\ kmol^{-1}\ s^{-1}$) and the components within the LCO lump into naphtha ($1.0\ 10^{-3}\ m^3\ kg_{cat}^{-1}\ s^{-1}$). The similarities among the rest of the kinetic parameters for the different catalysts lie in the synergistic and parallel effects of the porosity and acidity that boost the extent of the cracking reactions.

The values computed for the apparent activation energy of the different catalytic steps have been collected in Table 6. Unlike the kinetic parameters (Table 5), significant differences are observed between the activation energy required in some of the catalytic steps for the different catalysts. Likewise, the energy barrier that must be overcome for the deactivation step is very different depending on the catalyst used. The lower activation energy of the deactivation stage ($79.2\ kJ\ mol^{-1}$), added to the high value of the deactivation kinetic parameter obtained ($3.0\ 10^{-2}\ s^{-1}$ in Table 5) expose the high tendency of ECAT-2 to be deactivated. Equally, the high amount of acid sites on ECAT-3 explains the low activation energy required for the steps of formation of dry gas from HCO and LPG lumps (17.1 and 40.0 kJ mol^{-1}, respectively). In addition, the high matrix mesoporosity of ECAT-3, which is the other key feature of the catalysts, reduces the activation energy of the steps limited by the diffusivity of the components. This way, this catalyst reduces the energy involved in the steps that convert the HCO in LCO, LCO in naphtha and LCO in LPG (60.5, 42.5 and 58.3 kJ mol^{-1}, respectively), as well as in the formation of coke from LPG and dry gas (4.4 and 40.7 kJ mol^{-1}, respectively).

4.4. Yields of products

The evolution of the yields of products with high commercial interest as fuels (LCO and naphtha) and with high content of olefins (LPG) has been obtained for the three catalysts by computing the kinetic model previously described and using the kinetic parameters collected in Tables 5 and 6. One should note that the PPO fed to the reactor has a content of 12.5 wt% of LCO and a 5.5 wt% of naphtha, as it has been previously detailed in Section 4.1. Those contents have not been taken into account for depicting the evolution of the yields, in order to assess the formation of these lumps in its real magnitude. On the other hand, in order to fully understand the obtained results, it should be taken into account that conversion has been defined as the ratio of mass of HCO converted to lighter products and to coke to the mass of HCO fed:

$$\text{Conversion} = \frac{(m_{HCO})_{PPO} - (m_{HCO})_{Products}}{(m_{HCO})_{PPO}}\ 100 \tag{12}$$

The yield of each *i* lump of products has been defined as the mass of lump *i* referred to the total mass of lump HCO fed:

$$\text{Yield}_i = \frac{m_i}{m_{HCO}}\ 100 \tag{13}$$

Therefore, Figs. 2-4 compare the evolution with conversion of the yield of LCO, naphtha and LPG, respectively, obtained with the three catalysts at different temperatures. In a previous work [19] it has been detailed the composition of these lumps, stressing out the interest of the naphtha lump (research octane number up to 105) for being added to the stream of gasoline in refinery. It is also remarkable the propylene-rich LPG lump produced.

The trend of the curves in Fig. 2 exposes the character of the LCO lump as an intermediate in the reaction network [53], as they go through a maximum at values of conversion of ca. 80 wt%. Furthermore, it can be seen that high temperatures promote the cracking reactions that convert the molecules within this lump into lighter molecules,

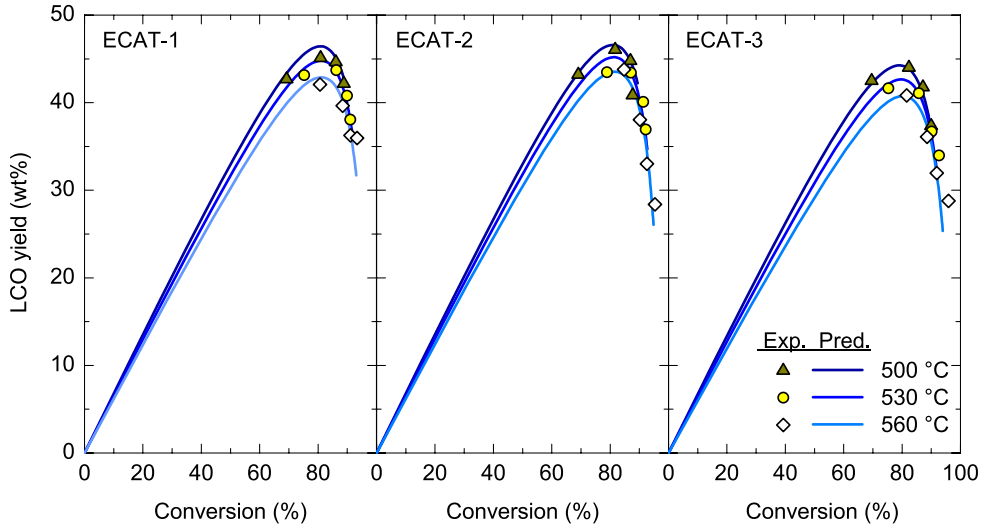

Fig. 2. Model prediction (lines) and experimental data (symbols) of the evolution of the LCO yield with the level of conversion for the three catalysts.

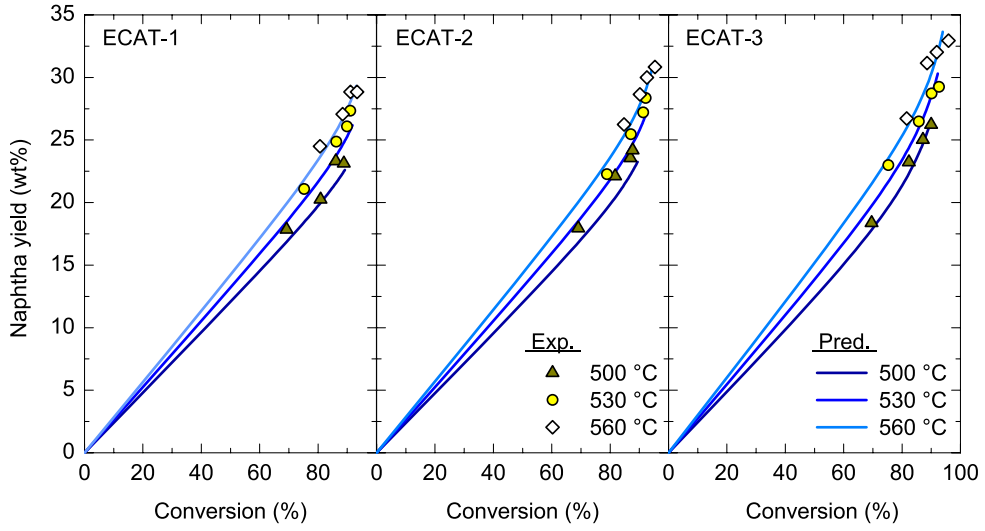

Fig. 3. Model prediction (lines) and experimental data (symbols) of the evolution of the naphtha yield with the level of conversion for the three catalysts.

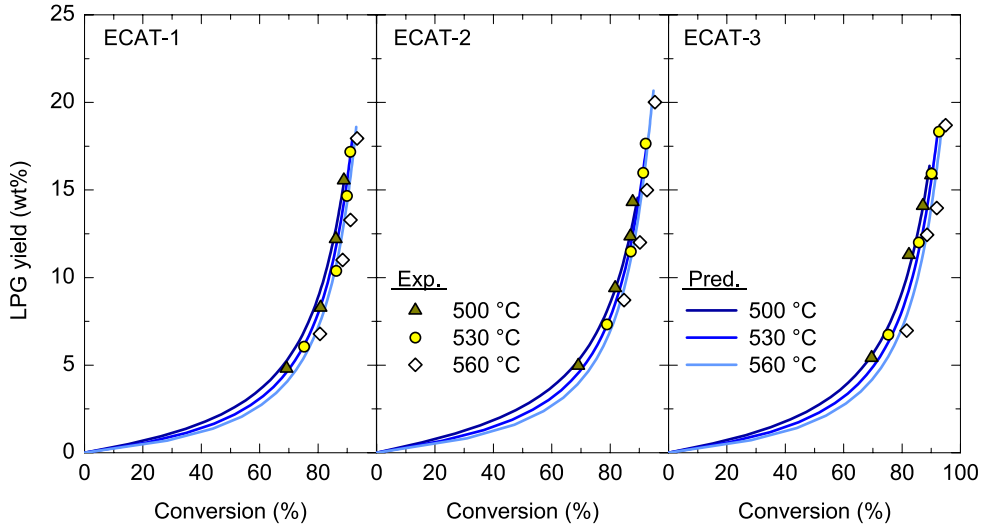

Fig. 4. Model prediction (lines) and experimental data (symbols) of the evolution of the LPG yield with the level of conversion for the three catalysts.

resulting in lower yields of LCO. Comparing the results obtained with the three catalysts, similarities are observed between the results obtained. This way, with ECAT-1 and ECAT-2 higher values than with ECAT-3 are obtained, yielding up to 46.5 wt% with the former catalysts at 500 °C.

Attending to the evolution of the yields of naphtha and LPG lumps (Figs. 3 and 4, respectively), both are end-products in the reaction network since their yield increases continuously with the extent of conversion. Nonetheless, in spite of the evolution obtained for LPG lump (Fig. 4), the molecules within this lump are cracked to dry gas and condensed to coke as it has been previously obtained in the reaction network (Fig. 1d). With regard to the evolution of the yield of naphtha (Fig. 3), high temperatures promote the production of this lump, since the cracking of molecules within HCO and LCO lumps is boosted. Furthermore, higher yields of naphtha have been obtained with ECAT-3, yielding up to 33.6 wt% at 560 °C. However, the maximum values obtained with ECAT-2 and ECAT-1 have been slightly inferiors (31.1 and 29.6 wt%, respectively).

The evolution of the different yields (Figs. 2-4) strongly depends on the properties of the catalyst used (Table 2) and can be correlated with the values of the apparent kinetic parameters reported on Table 5. This way, ECAT-3 is by far the catalyst with the highest and strongest acidity (124 $\mu mol_{NH3}\ g^{-1}$ and 130 kJ mol_{NH3}^{-1}, respectively), which turns into the catalyst with the highest cracking activity. Moreover, it is the catalyst with the highest mesoporosity that eases the access of the bulky molecules within the HCO and LCO lumps to the acid sites located in the inside of the porous structure of the catalyst. Therefore, the highest yields of naphtha and LPG, together with the lowest yield of LCO should be expected using this catalyst.

Even though ECAT-2 possesses a lower amount of acid sites available (81 $\mu mol_{NH3}\ g^{-1}$), their strength is quite remarkable (126 kJ mol_{NH3}^{-1}) making a priori this catalyst a serious candidate for maximizing the yield of naphtha and LPG lumps. However, its microporous nature and its, subsequent, shortness in mesopores are unsuitable for boosting the access of the heavy molecules to inner acid sites. Consequently, the behavior of ECAT-2 is only comparable with ECAT-3 at 560 °C as an increase in temperature increases the diffusivity [54]. Nonetheless, ECAT-2 promotes the formation of LPG instead of naphtha, which can be attributed to the overcracking reaction that takes place within the micropores of the zeolite as a consequence of the higher residence time of the reactants. Its low content of rare earths will also presumably contribute to obtain the aforementioned results [46]. Furthermore, the narrower porous structure of ECAT-2 will lead to a faster activity decay of the catalyst.

Finally, the configuration and composition of ECAT-1 are the less favorable ones to promote the cracking reactions. Indeed, ECAT-1 has the lowest superficial area (124 $m^2\ g^{-1}$), the lowest acidity (40 $\mu mol_{NH3}\ g^{-1}$) and the weakest acid strength (100 kJ mol_{NH3}^{-1}). In addition, the high concentration of impurity metals detected on ECAT-1, especially of vanadium (3335 ppm), will also contribute to deteriorate the properties of the catalyst. Consequently, slightly lower yields of both naphtha and LPG lumps (Figs. 3 and 4) have been obtained with ECAT-1.

4.5. Selectivity to products

The selectivity to each lump *i* has been defined as the mass of lump *i* formed respect to that of all the products:

$$\text{Selectivity}_i = \frac{m_i}{m_{LCO} + m_{Naphtha} + m_{LPG} + m_{DryGas} + m_{Coke}}\ 100 \qquad (14)$$

Taking into account that naphtha and LPG lumps are the ones with the highest commercial interest, the evolution with conversion of the selectivity to them has been depicted in Fig. 5. Overall, it can be seen how different the selectivity to each lump is. This way, the selectivity to naphtha lump is barely affected by the extent of conversion. The trend followed by the selectivity to naphtha curves depends on the catalyst. This way, it can be seen that with ECAT-1, which is the less active catalysts, the selectivity to naphtha remains almost steady for values of conversion below 80%, to increase exponentially at higher values. For ECAT-3, in turn, the growth can be noticed for values of conversion above 55%. Furthermore, the differences between the performances of the catalysts are more evident at high temperatures and high values of conversion. This way, the selectivity to naphtha has been maximized at 560 °C with ECAT-3 reaching a value of 35.8 wt%, whereas under the same conditions a selectivity of 31.5 wt% has been obtained with ECAT-1. ECAT-2, in turn, offers an intermediate result and a selectivity to naphtha of 32.8 wt%.

In contrast, selectivity to LPG lump grows exponentially with conversion since the very beginning of the reaction. The effect of the temperature is less marked but the opposite in the case of the LPG. Likewise, an increase from 500 to 560 °C for a fixed value of conversion entails just a reduction of the selectivity to LPG of ca. 2.5 wt%. Focusing on the performance of the catalysts, ECAT-2 offers the highest selectivity at 560 °C but also the lowest at 530 and 500 °C. This result is characteristic of a partially deactivated catalyst, in which thermal cracking plays a more important role that in the case of ECAT-1 and ECAT-3.

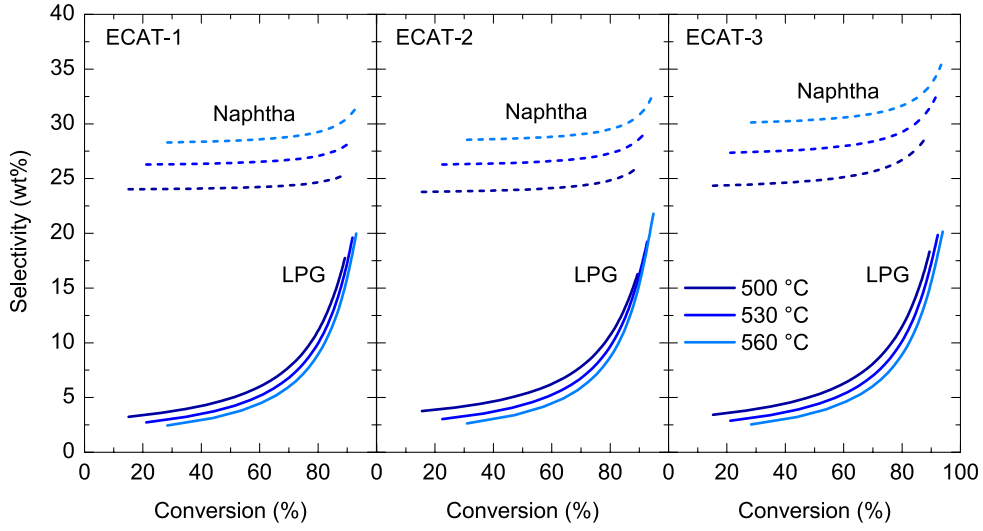

Fig. 5. Model prediction of the evolution of the selectivity to naphtha (dashed lines) and to LPG (solid lines) lumps with the level of conversion for the three catalysts.

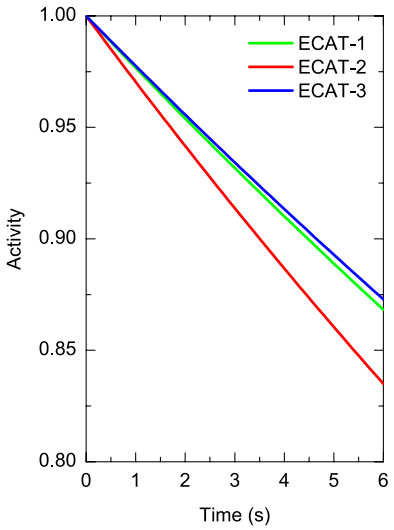

Fig. 6. Model prediction of the evolution of the catalysts activity with contact time at 500 °C.

Attending to the results collected on Figs. 2-5, operating under the conditions that allow for reaching conversions levels within the range 60–80% would be the optimal considering the possibility of varying the reaction temperature between 500 and 560 °C. This way, the conversion of HCO would be promoted keeping under control the overcracking reactions that would lead to obtain too much dry gas. Furthermore, ECAT-3 should be the selected one for turning the production to LPG and naphtha lumps, whereas ECAT-1 and ECAT-2 would increase the yield of LCO lump in detriment to the yield of naphtha.

4.6. Catalyst deactivation

Since catalyst deactivation has a notable impact on the results collected in Sections 4.4 and 4.5 about the yields and selectivity, the evolution of the activity term (φ) of the three catalysts with contact time at 500 °C has been plotted on Fig. 6. One should note that these curves have been obtained by applying the previously proposed deactivation equation (Eq. (7)) and using the corresponding kinetic parameters (Tables 5 and 6). It can be seen that for a contact time of 6 s, all the catalysts maintain good activity levels as they are above of the 83% of the initial activity. This result is very different to that obtained in the cracking of VGO (benchmark feed in FCC) [55], where the catalyst was totally deactivated. This result exposes the crucial role that the composition of the stream fed to cracking reactor plays in catalyst deactivation and, therefore, in products yield and distribution. This way, the heterogeneity of the VGO, with high contents of aromatics and the presence of polyaromatics, is more prone to the formation of coke than the olefins that predominate in the composition of the PPO [43]. This low deactivation is an interesting result for adopting different cracking strategies for the PPO, such as being co-fed with other refinery streams that deactivate the catalysts in a large extent.

Comparing the evolution followed by the catalysts, ECAT-1 and ECAT-3 show almost identical curves of activity vs. time as a difference of<1% for a contact time of 6 s (ca. 87%) has been obtained. However, ECAT-2 suffers from a higher and more severe activity decay since the very beginning of the reaction. Indeed, the final value for activity obtained for this latter catalyst is of 83.5%. Undoubtedly, the deactivation suffered by ECAT-2 lies in the porous structure of the catalyst, which is by far more microporous (Table 2) than the structure of the other catalysts. Consequently, the coke formed during the reaction will more easily block the channels of the zeolite reducing the accessibility of hydrocarbon species to the catalyst inner micropore network [56].

To offer another perspective of the deactivation results, Fig. 7 depicts the evolution of the activity of the three catalysts with the content of coke deposited. Clearly, the amount of coke deposited on ECAT-2 is higher than that deposited on ECAT-1 or ECAT-3. Consequently, ECAT-2 suffers from a higher activity decay than the other catalysts. In spite of that, attending to the accelerated decrease of the activity obtained for all the catalysts, it can be concluded that the deactivation mechanism is highly affected by the micropore blocking caused by coke deposition. This phenomenon will also restrict the access of the reactants to the acid sites located in the inner crystals of the zeolite. This result is in concordance with the hypothesis of the key role of the matrix mesopores for attenuating the catalyst deactivation by delaying the aforementioned phenomenon.

5. Conclusions

A lumped kinetic modeling method has been applied to the experimental data of the catalytic cracking of plastic pyrolysis oil (PPO) over three commercial FCC equilibrium catalysts. By means of a statistical data analysis, it has been obtained that from the four different reaction networks proposed, the simplest one was the most appropriate for describing the process. From the kinetic parameters obtained in the fitting of the results, it has been obtained that both total acidity and acid

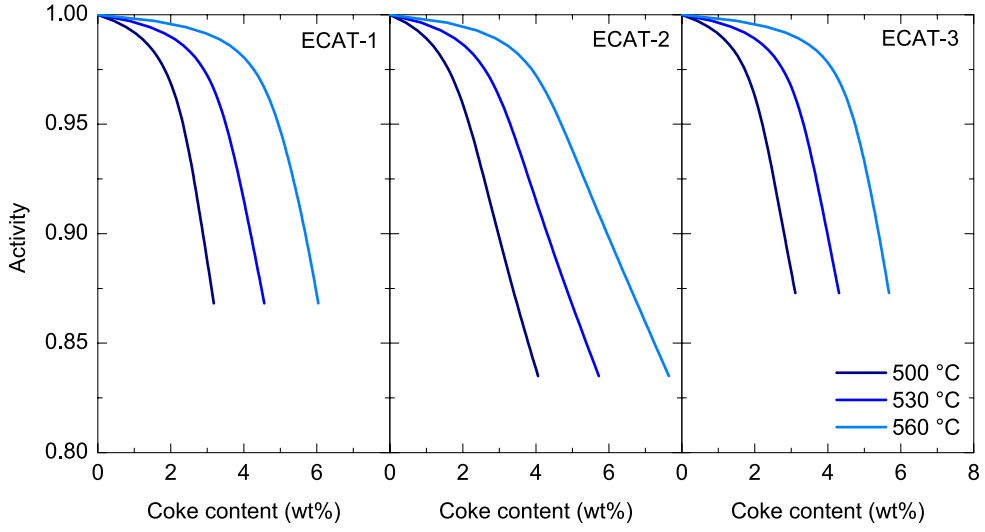

Fig. 7. Model prediction of the evolution of the catalyst activity with the content of coke deposited on the three catalysts.

strength rule the cracking process, boosting the extent of the different reaction steps and modifying the distribution of the lumps of products. Furthermore, the mesoporous structure of the matrix is a key feature for reducing the diffusional restrictions and, subsequently, for maximizing the formation of the naphtha and LPG lumps. This way, the maximum yield and selectivity to naphtha of 33.6 and 35.8 wt%, respectively, have been obtained with ECAT-3 for a conversion value of 94%. In contrast, ECAT-1 and ECAT-2 promote the formation of LCO instead of naphtha.

The deactivation of the three catalysts in the cracking of the PPO is by far lower than that obtained in the cracking of VGO (benchmark feedstock of FCC unit), because of the absence of aromatics in the PPO. Likewise, for a contact time of 6 s the catalysts keep a residual activity above the 80%. The lowest deactivation of ECAT-3 ($k_d = 2.3\ 10^{-2}\ s^{-1}$) has been related to the high mesoporosity of its matrix, which is appropriate for promoting the internal diffusion of coke precursors, attenuating the catalyst deactivation. This way, for this catalyst, the apparent activation energies of the conversion of heavy cycle oil (HCO) into light cycle oil (LCO), LCO into naphtha, and LCO into liquefied petroleum gases (LPG) are 60.5 42.5 and 58.3 kJ mol^{-1}, respectively. In addition, those of the formation of coke from HCO, LPG and dry gas are 129.0, 4.4 and 40.7 kJ mol^{-1}, respectively.

The kinetic model proposed is an interesting tool for facing the manufacturing of reactors designed *ad hoc* for the catalytic cracking of PPO. Additionally, obtained results could also encourage the future co-feeding of this alternative and waste-derived feedstock to industrial FCC units commonly available in oil refineries. Nevertheless, the kinetic results could be modified by the presence of additives and pollutants in the waste plastics.

CRediT authorship contribution statement

Roberto Palos: Formal analysis, Conceptualization, Writing – original draft. **Elena Rodríguez:** Investigation, Formal analysis. **Alazne Gutiérrez:** Supervision, Methodology, Visualization. **Javier Bilbao:** Conceptualization, Writing – review & editing, Supervision, Project administration, Funding acquisition. **José M. Arandes:** Software, Resources, Project administration, Funding acquisition.

Declaration of Competing Interest

The authors declare that they have no known competing financial interests or personal relationships that could have appeared to influence the work reported in this paper.

Acknowledgments

This work has been carried out with the financial support of the Ministry of Science, Innovation and Universities (MICIU) of the Spanish Government (grant RTI2018-096981-B-I00), the European Union's ERDF funds and Horizon 2020 research and innovation programme under the Marie Skłodowska-Curie Actions (grant No 823745) and the Basque Government (grant IT1218-19). Dr. Roberto Palos thanks the University of the Basque Country UPV/EHU for his postdoctoral grant (UPV/EHU 2019). The authors also acknowledge Petronor Refinery for providing with the catalyst used in this work.

Appendix A. Supplementary data

Supplementary data to this article can be found online at https://doi.org/10.1016/j.fuel.2022.123341.

References

[1] Cook CR, Halden RU. Ecological and health issues of plastic waste. Plast Waste Recycl, Elsevier; 2020, p. 513–27. https://doi.org/10.1016/b978-0-12-817880-5.00020-7.

[2] Lopez G, Artetxe M, Amutio M, Bilbao J, Olazar M. Thermochemical routes for the valorization of waste polyolefinic plastics to produce fuels and chemicals. A review. Renew Sustain Energy Rev 2017;73:346–68. https://doi.org/10.1016/j.rser.2017.01.142.

[3] Wong SL, Ngadi N, Abdullah TAT, Inuwa IM. Current state and future prospects of plastic waste as source of fuel: A review. Renew Sustain Energy Rev 2015;50:1167–80. https://doi.org/10.1016/j.rser.2015.04.063.

[4] Owusu PA, Banadda N, Zziwa A, Seay J, Kiggundu N. Reverse engineering of plastic waste into useful fuel products. J Anal Appl Pyrol 2018;130:285–93. https://doi.org/10.1016/j.jaap.2017.12.020.

[5] Artetxe M, Lopez G, Amutio M, Barbarias I, Arregi A, Aguado R, et al. Styrene recovery from polystyrene by flash pyrolysis in a conical spouted bed reactor. Waste Manage 2015;45:126–33. https://doi.org/10.1016/j.wasman.2015.05.034.

[6] Lopez G, Artetxe M, Amutio M, Elordi G, Aguado R, Olazar M, et al. Recycling poly-(methyl methacrylate) by pyrolysis in a conical spouted bed reactor. Chem Eng Process Process Intensif 2010;49(10):1089–94. https://doi.org/10.1016/j.cep.2010.08.002.

[7] Vela FJ, Palos R, Trueba D, Bilbao J, Arandes JM, Gutiérrez A. Different approaches to convert waste polyolefins into automotive fuels via hydrocracking with a NiW/HY catalyst. Fuel Process Technol 2021;220:106891. https://doi.org/10.1016/j.fuproc.2021.106891.

[8] Qureshi MS, Oasmaa A, Pihkola H, Deviatkin I, Tenhunen A, Mannila J, et al. Pyrolysis of plastic waste: opportunities and challenges. J Anal Appl Pyrol 2020;152:104804. https://doi.org/10.1016/j.jaap.2020.104804.

[9] Kunwar B, Chandrasekaran SR, Moser BR, Deluhery J, Kim P, Rajagopalan N, et al. Catalytic thermal cracking of postconsumer waste plastics to fuels. 2. Pilot-scale thermochemical conversion. Energy Fuels 2017;31(3):2705–15. https://doi.org/10.1021/acs.energyfuels.6B02996.

[10] Gala A, Guerrero M, Guirao B, Domine ME, Serra JM. Characterization and distillation of pyrolysis liquids coming from polyolefins segregated of MSW for their use as automotive diesel fuel. Energy Fuels 2020;34(5):5969–82. https://doi.org/10.1021/acs.energyfuels.0c00403.

[11] Palos R, Gutiérrez A, Vela FJ, Olazar M, Arandes JM, Bilbao J. Waste refinery: the valorization of waste plastics and end-of-life tires in refinery units. A review. Energy Fuels 2021;35(5):3529–57. https://doi.org/10.1021/acs.energyfuels.0c03918.

[12] Palos R, Gutiérrez A, Fernández ML, Trueba D, Bilbao J, Arandes JM. Upgrading of heavy coker naphtha by means of catalytic cracking in refinery FCC unit. Fuel Process Technol 2020;205:106454. https://doi.org/10.1016/j.fuproc.2020.106454.

[13] Palos R, Gutiérrez A, Fernández ML, Azkoiti MJ, Bilbao J, Arandes JM. Converting the surplus of low-quality naphtha into more valuable products by feeding it to a fluid catalytic cracking unit. Ind Eng Chem Res 2020;59(38):16868–75. https://doi.org/10.1021/acs.iecr.0c03257.

[14] Ibarra Á, Rodríguez E, Sedran U, Arandes JM, Bilbao J. Synergy in the cracking of a blend of bio-oil and vacuum gasoil under fluid catalytic cracking conditions. Ind Eng Chem Res 2016;55(7):1872–80. https://doi.org/10.1021/acs.iecr.5b04502.

[15] Arabiourrutia M, Elordi G, Lopez G, Borsella E, Bilbao J, Olazar M. Characterization of the waxes obtained by the pyrolysis of polyolefin plastics in a conical spouted bed reactor. J Anal Appl Pyrol 2012;94:230–7. https://doi.org/10.1016/j.jaap.2011.12.012.

[16] Elordi G, Olazar M, Lopez G, Amutio M, Artetxe M, Aguado R, et al. Catalytic pyrolysis of HDPE in continuous mode over zeolite catalysts in a conical spouted bed reactor. J Anal Appl Pyrol 2009;85(1-2):345–51. https://doi.org/10.1016/j.jaap.2008.10.015.

[17] Renzini MS, Sedran U, Pierella LB. H-ZSM-11 and Zn-ZSM-11 zeolites and their applications in the catalytic transformation of LDPE. J Anal Appl Pyrol 2009;86(1):215–20. https://doi.org/10.1016/j.jaap.2009.06.008.

[18] Elordi G, Olazar M, Artetxe M, Castaño P, Bilbao J. Effect of the acidity of the HZSM-5 zeolite catalyst on the cracking of high density polyethylene in a conical spouted bed reactor. Appl Catal A Gen 2012;415–416:89–95. https://doi.org/10.1016/j.apcata.2011.12.011.

[19] Rodríguez E, Palos R, Gutiérrez A, Vela FJ, Arandes JM, Bilbao J. Effect of the FCC equilibrium catalyst properties and of the cracking temperature on the production of fuel from HDPE pyrolysis waxes. Energy Fuels 2019;33(6):5191–9. https://doi.org/10.1021/acs.energyfuels.9b00993.

[20] Dupain X, Krul RA, Schaverien CJ, Makkee M, Moulijn JA. Production of clean transportation fuels and lower olefins from Fischer-Tropsch synthesis waxes under fluid catalytic cracking conditions: The potential of highly paraffinic feedstocks for FCC. Appl Catal B Environ 2006;63(3-4):277–95. https://doi.org/10.1016/j.apcatb.2005.10.012.

[21] Yang M, Zhang L, Wang G, Chen Z, Han J, Gao C, et al. Fischer-Tropsch wax catalytic cracking for the production of low olefin and high octane number gasoline: experiment and molecular level kinetic modeling study. Fuel 2021;303:121226. https://doi.org/10.1016/j.fuel.2021.121226.

[22] Moustafa TM, Froment GF. Kinetic modeling of coke formation and deactivation in the catalytic cracking of vacuum gas oil. Ind Eng Chem Res 2003;42(1):14–25. https://doi.org/10.1021/ie0204538.

[23] Gao H, Wang G, Xu C, Gao J. Eight-lump kinetic modeling of vacuum residue catalytic cracking in an independent fluid bed reactor. Energy Fuels 2014;28(10):6554–62. https://doi.org/10.1021/ef501260N.

[24] Sani AG, Ebrahim HA, Azarhoosh MJ. 8-Lump kinetic model for fluid catalytic cracking with olefin detailed distribution study. Fuel 2018;225:322–35. https://doi.org/10.1016/j.fuel.2018.03.087.

[25] John YM, Mustafa MA, Patel R, Mujtaba IM. Parameter estimation of a six-lump kinetic model of an industrial fluid catalytic cracking unit. Fuel 2019;235:1436–54. https://doi.org/10.1016/j.fuel.2018.08.033.
[26] den Hollander MA, Makkee M, Moulijn JA. Coke formation in fluid catalytic cracking studied with the microriser. Catal Today 1998;46(1):27–35. https://doi.org/10.1016/S0920-5861(98)00348-4.
[27] Occelli ML, Olivier JP, Auroux A. The location and effects of coke deposition in fluid cracking catalysts during gas oil cracking at microactivity test conditions. J Catal 2002;209(2):385–93. https://doi.org/10.1006/jcat.2002.3639.
[28] Afshar Ebrahimi A, Mousavi H, Bayesteh H, Towfighi J. Nine-lumped kinetic model for VGO catalytic cracking; using catalyst deactivation. Fuel 2018;231:118–25. https://doi.org/10.1016/j.fuel.2018.04.126.
[29] Zhao X, Sun S. Lumped kinetic modeling method for fluid catalytic cracking. Chem Eng Technol 2020;43(12):2493–500. https://doi.org/10.1002/ceat.202000277.
[30] Al-Sabawi M, Atias JA, de Lasa H. Heterogeneous approach to the catalytic cracking of vacuum gas oil. Ind Eng Chem Res 2008;47(20):7631–41. https://doi.org/10.1021/ie701745k.
[31] Orozco S, Alvarez J, Lopez G, Artetxe M, Bilbao J, Olazar M. Pyrolysis of plastic wastes in a fountain confined conical spouted bed reactor: determination of stable operating conditions. Energy Convers Manage 2021;229:113768. https://doi.org/10.1016/j.enconman.2020.113768.
[32] Jiménez-García G, Aguilar-López R, León-Becerril E, Maya-Yescas R. Tracking catalyst activity during fluidized-bed catalytic cracking. Ind Eng Chem Res 2009;48(3):1220–7. https://doi.org/10.1021/ie800650y.
[33] De Lasa H. Riser Simulator, U.S. Patent. 5,102,628, 1992.
[34] Rodríguez E, Gutiérrez A, Palos R, Azkoiti MJ, Arandes JM, Bilbao J. Cracking of scrap tires pyrolysis oil in a fluidized bed reactor under catalytic cracking unit conditions. Effects of operating conditions. Energy Fuels 2019;33(4):3133–43. https://doi.org/10.1021/acs.energyfuels.9b00292.
[35] Toch K, Thybaut JW, Marin GB. A systematic methodology for kinetic modeling of chemical reactions applied to n-hexane hydroisomerization. AIChE J 2015;61(3):880–92. https://doi.org/10.1002/aic.14680.
[36] Cordero-Lanzac T, Aguayo AT, Gayubo AG, Castaño P, Bilbao J. Simultaneous modeling of the kinetics for n-pentane cracking and the deactivation of a HZSM-5 based catalyst. Chem Eng J 2018;331:818–30. https://doi.org/10.1016/j.cej.2017.08.106.
[37] Cordero-Lanzac T, Aguayo AT, Castaño P, Bilbao J. Kinetics and reactor modeling of the conversion of n-pentane using HZSM-5 catalysts with different Si/Al ratios. React Chem Eng 2019;4(11):1922–34. https://doi.org/10.1039/c9re00222g.
[38] Palos R, Rodríguez E, Gutiérrez A, Bilbao J, Arandes JM. Kinetic modeling for the catalytic cracking of tires pyrolysis oil. Fuel 2022;309:122055. https://doi.org/10.1016/j.fuel.2021.122055.
[39] Al Jamri M, Li J, Smith R. Molecular modeling of coprocessing biomass fast pyrolysis oil in fluid catalytic cracking unit. Ind Eng Chem Res 2020;59(5):1989–2004. https://doi.org/10.1021/acs.iecr.9b05361.
[40] Gupta RK, Kumar V, Srivastava VK. Modeling of fluid catalytic cracking riser reactor: a review. Int J Chem React Eng 2010;8. https://doi.org/10.2202/1542-6580.2334.
[41] Palos R, Gutiérrez A, Hita I, Castaño P, Thybaut JW, Arandes JM, et al. Kinetic modeling of hydrotreating for enhanced upgrading of light cycle oil. Ind Eng Chem Res 2019;58(29):13064–75. https://doi.org/10.1021/acs.iecr.9b02095.
[42] Rodríguez E, Palos R, Gutiérrez A, Trueba D, Arandes JM, Bilbao J. Towards waste refinery: co-feeding HDPE pyrolysis waxes with VGO into the catalytic cracking unit. Energy Convers Manage 2020;207:112554. https://doi.org/10.1016/j.enconman.2020.112554.
[43] Rodríguez E, Gutiérrez A, Palos R, Vela FJ, Arandes JM, Bilbao J. Fuel production by cracking of polyolefins pyrolysis waxes under fluid catalytic cracking (FCC) operating conditions. Waste Manage 2019;93:162–72. https://doi.org/10.1016/j.wasman.2019.05.005.
[44] Rodríguez E, Palos R, Gutiérrez A, Arandes JM, Bilbao J. Production of non-conventional fuels by catalytic cracking of scrap tires pyrolysis oil. Ind Eng Chem Res 2019;58(13):5158–67. https://doi.org/10.1021/acs.iecr.9b00632.
[45] Vogt ETC, Weckhuysen BM. Fluid catalytic cracking: recent developments on the grand old lady of zeolite catalysis. Chem Soc Rev 2015;44(20):7342–70. https://doi.org/10.1039/c5cs00376h.
[46] Akah A. Application of rare earths in fluid catalytic cracking: a review. J Rare Earths 2017;35(10):941–56. https://doi.org/10.1016/s1002-0721(17)60998-0.
[47] Etim UJ, Bai P, Liu X, Subhan F, Ullah R, Yan Z. Vanadium and nickel deposition on FCC catalyst: Influence of residual catalyst acidity on catalytic products. Microporous Mesoporous Mater 2019;273:276–85. https://doi.org/10.1016/j.micromeso.2018.07.011.
[48] Chuzlov V, Nazarova G, Ivanchina E, Ivashkina E, Dolganova I, Solopova A. Increasing the economic efficiency of gasoline production: reducing the quality giveaway and simulation of catalytic cracking and compounding. Fuel Process Technol 2019;196:106139. https://doi.org/10.1016/j.fuproc.2019.106139.
[49] Guisnet M, Costa L, Ribeiro FR. Prevention of zeolite deactivation by coking. J Mol Catal A: Chem 2009;305(1-2):69–83. https://doi.org/10.1016/j.molcata.2008.11.012.
[50] Ibáñez M, Pérez-Uriarte P, Sánchez-Contador M, Cordero-Lanzac T, Aguayo A, Bilbao J, et al. Nature and location of carbonaceous species in a composite HZSM-5 zeolite catalyst during the conversion of dimethyl ether into light olefins. Catalysts 2017;7(9):254. https://doi.org/10.3390/catal7090254.
[51] Cordero-Lanzac T, Ateka A, Pérez-Uriarte P, Castaño P, Aguayo AT, Bilbao J. Insight into the deactivation and regeneration of HZSM-5 zeolite catalysts in the conversion of dimethyl ether to olefins. Ind Eng Chem Res 2018;57(41):13689–702. https://doi.org/10.1021/acs.iecr.8B03308.
[52] Díaz M, Epelde E, Valecillos J, Izaddoust S, Aguayo AT, Bilbao J. Coke deactivation and regeneration of HZSM-5 zeolite catalysts in the oligomerization of 1-butene. Appl Catal B Environ 2021;291:120076. https://doi.org/10.1016/j.apcatb.2021.120076.
[53] Al-Absi AA, Aitani AM, Al-Khattaf SS. Thermal and catalytic cracking of whole crude oils at high severity. J Anal Appl Pyrol 2020;145:104705. https://doi.org/10.1016/j.jaap.2019.104705.
[54] Zheng J, Zhang H, Liu Y, Wang G, Kong Q, Pan M, et al. Synthesis of wool-ball-like ZSM-5 with enlarged external surfaces and improved diffusion: a potential highly-efficient FCC catalyst component for elevating pre-cracking of large molecules and catalytic longevity. Catal Lett 2016;146(8):1457–69. https://doi.org/10.1007/s10562-016-1776-8.
[55] Cerqueira HS, Caeiro G, Costa L, Ramôa Ribeiro F. Deactivation of FCC catalysts. J Mol Catal A: Chem 2008;292(1-2):1–13. https://doi.org/10.1016/j.molcata.2008.06.014.
[56] Jiménez-García G, De Lasa H, Quintana-Solórzano R, Maya-Yescas R. Catalyst activity decay due to pore blockage during catalytic cracking of hydrocarbons. Fuel 2013;110:89–98. https://doi.org/10.1016/j.fuel.2012.10.082.